Formation of Bubbles, Blobs, and Surface Cusps in Complex Plasmas

M. Schwabe,* M. Rubin-Zuzic, S. Zhdanov, A. V. Ivlev, H. M. Thomas, and G. E. Morfill

Max-Planck-Institut für extraterrestrische Physik, D-85748 Garching, Germany

(Received 3 December 2008; published 26 June 2009)

Investigations of the dynamical evolution of a complex plasma, in which a vertical temperature gradient compensates gravity, were carried out. At low power the formation of microparticle bubbles, blobs, and spraying cusps was observed. This activity can be turned on and off by changing control parameters, such as the rf power and the gas pressure. Several observational effects indicate the presence of surface tension, even at small "nanoscales" of a few 100's of particles. By tracing the individual microparticle motion the detailed (atomistic) dynamics can be studied as well as the pressure dependence of the forces. A possible mechanism that could drive the observed phenomena is analogous to the Rayleigh-Taylor instability.

DOI: 10.1103/PhysRevLett.102.255005 PACS numbers: 52.27.Lw, 52.35.Py

The behavior of liquid drops in an air stream and that of a blob of sedimenting (mesoscopic) particles in a liquid has been investigated in numerous experiments [1,2]. Depending on the Weber number $\mathcal{W}$ of the system (the ratio of inertia to surface tension forces) different breakup mechanisms are possible [3]. For low $\mathcal{W}$, for example, bag breakup is likely: the drop first deforms into a bag shape, then bursts in the center. For intermediate $\mathcal{W}$, one probable breakup mechanism is sheet stripping, where particles are emitted from the sides of the drop, forming pointed edges. At high $\mathcal{W}$, catastrophic breakup and wave crest stripping can occur, whereby the drop disintegrates on the sides [3].

Sedimentation studies are used to investigate the movement of single particles in an ensemble or blob. Their overall behavior is similar to water drops, depending on whether the particles are small enough that a continuum view is applicable. The analogy between these "suspension drops" and liquid drops is fundamental without interfacial tension needed. For instance, the drops form membranes when breaking up, show similar vortices as found inside water drops [2,4], and sometimes emit individual particles, forming a tail [5].

The complementary problem of bubbles in a fluidized bed is also of interest. An ensemble of particles is fluidized if its weight is completely supported by an upward flow of fluid [6]. When a gas is used, bubbles are formed frequently. The gas inside one of those bubbles moves in a vortex, pushing the particles out and forming an "empty" void [7]. The supporting gas can also be ionized, producing a plasma-fluidized particle bed. There have been investigations of strong coupling effects between the particles in a plasma-fluidized bed [8]. Many other similar systems exist, e.g., electron bubbles forming at the solid-superfluid interface of helium under the influence of an electric field [9] and the formation of conic cusps at the surface of liquid metal in electric fields [10].

A recently discovered system which can be used to study fluid phenomena is a complex plasma [11–13]: a low-temperature, low-pressure plasma with microparticles which acquire high negative charges and interact with each other. Microparticles can be visualized individually, so that fully resolved kinetic studies are possible. Bubbles in complex plasmas have been artificially produced [14] by ablating some microparticles with a strong laser pulse. The resulting plume pushed the microparticles outwards, creating a particle-free region (void).

Here we report the first observation of a spontaneous formation of microparticle blobs (drops), cusps, and bubbles in a complex plasma (Figs. 1(a)–1(c)]. The experiments were performed in the PK-3 Plus laboratory [15] under gravity conditions, as described in [16]. The plasma is produced in a capacitively coupled plasma chamber with

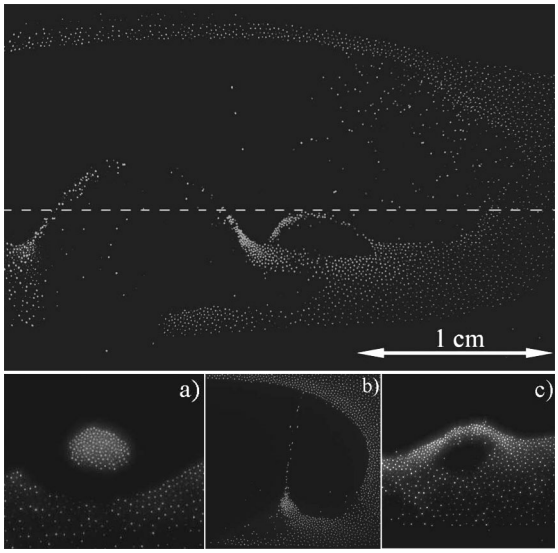

FIG. 1. Observed fluid activity in a complex plasma. Top: Two microparticle bubbles (6.81 μm particles, $\Delta T = 65$ K, argon plasma). The dashed line indicates the midplane of the plasma chamber. Bottom: (a) Microparticle blob [field of view (FoV) 8×7 mm^2, 6.8 μm particles]. (b) Microparticle spray (FoV 11×11 mm^2, 4.8 μm particles). (c) Microparticle bubble (FoV 9×9 mm^2, 6.8 μm particles). A movie showing bubbles, blobs, and cusps (FoV 29×19 mm^2, 6.8 μm particles, $\Delta T = 64.5$ K, Ar) is available online [21].

electrodes driven in push-pull mode and separated by 3 cm. Micrometer sized melamine formaldehyde particles with a mass density of 1510 kg/m^3 are inserted into the plasma via dispensers and are illuminated from the side with a vertically spread laser beam. The scattered light is recorded with a camera at a maximal frame rate of 1000 fps. The laser and the camera are mounted on a translation stage, which makes it possible to scan through the system horizontally with a velocity of up to 8 mm/s. The ground plate of the chamber is heated with evenly distributed resistors; the upper plate is cooled with two fans. This produces a temperature gradient in the chamber and thus an additional thermophoretic force upwards [17]. The temperature difference is measured at the ground plates. In rarefied gases, there is a temperature jump between the electrodes and the gas [18], which reduces the gas temperature gradient set in the chamber.

When gravity is approximately compensated by the thermophoretic force, we observe typical phenomena that also occur in complex plasmas under microgravity. These are the formation of a void in the center of the chamber, which is caused by the balance of ion drag and electrostatic forces acting on the microparticles [19], and microparticle vortex motions in the off axis region of the plasma chamber [20]. Further increase of the temperature gradient usually causes the microparticles to flow around the void to the top of the chamber.

Under certain conditions, when the rf power is low and the pressure is high, so that the plasma is close to turning off (power of the rf generator 45–55 mW, effective voltage on the electrodes 10–12 V, pressure between 18 and 45 Pa depending on the particle size and number density), the microparticle fluid starts to show remarkable behavior. First, the void becomes unstable, with microparticles moving through the void region from the bottom to the top. Similar behavior has also been observed under microgravity conditions in the PKE-Nefedov setup.

In our experiments, indentations and cusps in the lower void boundary become visible. The number density of the microparticles below the void is increased compared to the rest of the microparticle fluid. Estimates show that in this case the ''Havnes parameter'' can substantially exceed unity and hence the electron density can be strongly depleted. Unstable *bubbles* appear in the region below the void: entire layers of microparticles are pushed upwards into the void, forming blisters until the upper ''lid'' breaks up. Under the same conditions, we also observe *blobs*, which are self-contained microparticle droplets [see Fig. 1(a)], and *sprays* [see Fig. 1(b)], in which a narrow microparticle beam is ejected from a tip (*cusp*) into the void upwards (see also the video online [21]).

The microparticle motion inside a blob and during the formation of a bubble is shown in Fig. 2. Inside a blob, the microparticle motion forms vortices reminiscent of the motion observed inside a water drop [4]. In Fig. 2(b), the upward accelerated motion of the microparticles during the formation (also illustrated in Fig. 1(c)] of a bubble is visualized. Figure 2(b) also points to a formation mechanism of the blobs: At the later stages, the left part of the microparticle fluid is almost completely disconnected from the right part, resulting in a microparticle accumulation or blob. Blobs typically break up by emitting a stream of particles into the void, often in the shape of a chain of particles similar to the spray shown in Fig. 1. This is similar to sedimentation of particles in a fluid [5]. Blobs can also disintegrate, analogous to water drops in an air stream during wave crest stripping [3]. Fast horizontal scans through our system show that the particle blobs sometimes are indeed completely isolated. An example is shown in Fig. 3.

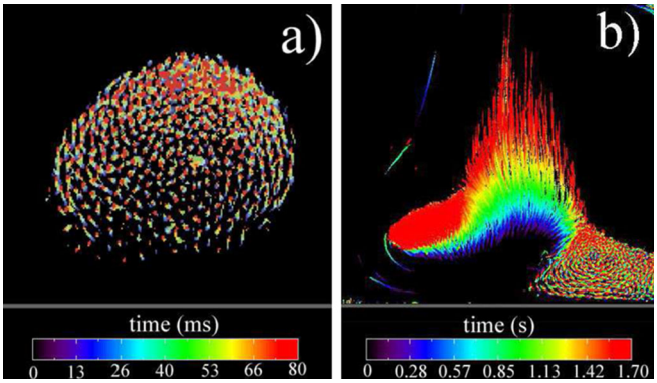

FIG. 2 (color online). Color-coded superposition of pictures demonstrating the movement of microparticles (a) inside a blob (FoV 4×4 mm^2, 7.2 μm particles, $\Delta T = 63$ K, argon plasma) and (b) while a bubble is forming (FoV 11×10 mm^2, 4.8 μm particles, $\Delta T = 49.5$ K, argon plasma).

While bubble activity occurs in a variety of experimental conditions (particles with diameters between 4.8 and 7.2 μm, argon and neon plasmas), it depends very strongly on control parameters (rf power, temperature gradient, pressure, particle number density). It can be switched on and off by changing any of those parameters. There is no detectable effect on discharge parameters such as effective voltage, current, and harmonics, when the instability starts, and there is no visible correlation of the plasma glow with the bubbles.

At higher temperature gradients a lower gas pressure suffices to trigger the appearance of bubbles (see the inset of Fig. 4). Furthermore, the amount of the microparticle fluid involved in this activity depends on the pressure: When the pressure is increased, the bubbles are formed closer to the lower edge of the particle cloud, until at some pressure the whole lower part of the microparticle cloud participates in the bubble formation. The reason for that could be a saturation in the thermophoretic force at low pressures observed in [17]. Even though sometimes a sudden change of a control parameter induces a transient bubble, the activity itself is not a transient phenomenon and can occur for a long time (more than an hour). In the case of stable bubble activity, microparticles which are pushed upwards flow back underneath the void from the sides.

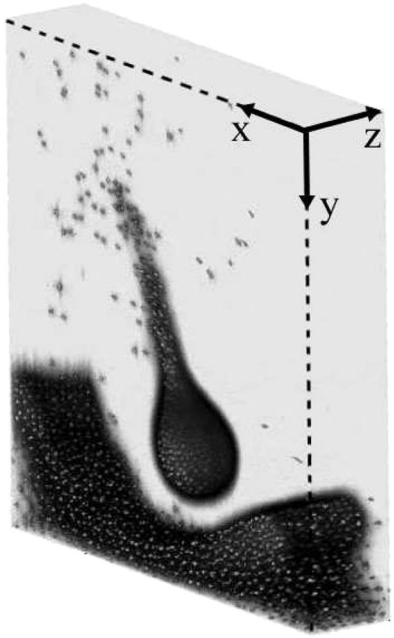

FIG. 3. Three-dimensional slice showing a particle blob (colors inverted, FoV $11 \times 2 \times 12$ mm^3, 6.8 μm particles, $\Delta T = 63.5$ K, argon plasma) recorded by horizontal scanning at a speed of 8 mm/s. The particles on the bottom correspond to the region below the void. Note the irregular structure of the void edge with indentations as mentioned in the text.

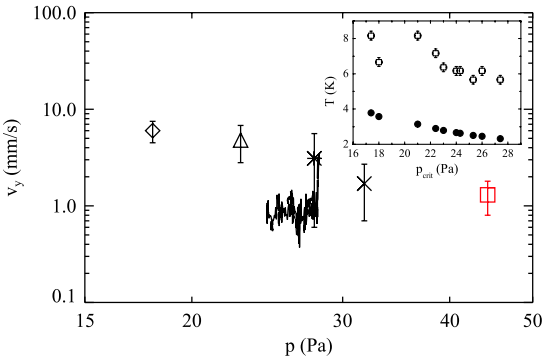

FIG. 4 (color online). Mean velocity of particles moving upwards versus gas pressure. The results correspond to different particle diameters $2a$ and temperature differences between the electrodes ΔT (diamond, triangle, star, and bold line are for $2a = 6.8$ μm, $\Delta T = 63$–64.5 K; cross and square are for $2a = 4.8$ μm, $\Delta T = 45$–48 K). The red square indicates measurements taken while the plasma was turned off. The bold line shows an experiment with a gradual pressure increase, in other experiments the pressure was kept constant. The error bars indicate the FWHM of the velocity distributions. Inset: Open symbols show the excess of the critical temperature needed for the appearance of bubbles (above the equilibrium temperature needed to compensate gravity [17]). Filled symbols show the total temperature jump between the electrodes and the gas predicted by [18] in the creep flow regime.

Often, but not always, there are several consecutive bubbles ejected at the same position.

Figure 4 shows the mean particle velocity near the midplane of the chamber as a function of gas pressure. It is smaller for small particles and decreases with pressure. This result excludes the Rayleigh-Bénard mechanism of gas convection as the cause for the particle movement (also, the Rayleigh number at such low pressures is 5–6 orders of magnitude below the critical number for Bénard convection [22]). A possible mechanism, which operates in rarefied gases, is thermal creep flow. This is induced in the direction of a temperature gradient along a wall [23,24], and its strength is inversely proportional to pressure. The inset in Fig. 4 shows the critical temperature for the appearance of bubbles as a function of pressure for experiments with 6.8 μm particles and the expected temperature jump for those conditions across the Knudsen layer [18]. Both temperatures decrease with pressure.

Let us now consider a phenomenological model that can explain the observed fluid activity. The void boundary is stabilized by the drag force exerted by ions drifting from the center of the chamber towards the edges. When the rf power is lowered or the pressure increased up to the point where the plasma is near turn-off conditions, this ion flux becomes very weak. The acceleration (induced by thermophoresis or creep flow) of the microparticle fluid into the void may then lead to the development of a Rayleigh-Taylor instability at the interface [22], resembling that occurring in colloids under the influence of gravity [25,26]. The instability in our experiments sometimes develops on a surface of rather thin "membranes" of thickness $H = 1$–3 mm. The observed characteristic wavelength of the most unstable mode is typically $\lambda_{\max} \equiv 2\pi/k_{\max} \sim 3$ mm. Hence $Hk_{\max} \geq 3$ and thus the "deep-water" regime is quite appropriate to describe the gravity-capillary waves. Our model depends on the acceleration of the destabilizing forces $\tilde{g}$ ("effective gravity," the sum of the forces exerted by thermophoresis, neutral gas flow, ion drag, and electric forces), the surface tension, α, the mass density of the microparticle cloud, ρ, and the damping rate coefficient γ. The resulting dispersion relation is: $\omega^2 + i\gamma\omega = -\tilde{g}k + (\alpha/\rho)k^3$. Therefore, we obtain

$$k_{\max} = \sqrt{\frac{\rho\tilde{g}}{3\alpha}}, \qquad \mathrm{Im}\omega_{\max} \simeq \sqrt{\frac{4\rho\tilde{g}^3}{27\alpha\gamma^2}}. \tag{1}$$

The typical observed value of the instability increment is about Im $\omega_{\max} \simeq 2$ s^{-1}, which is more than an order of magnitude smaller than $\gamma \simeq 50$ s^{-1}. Using this value and $\lambda_{\max}$ as observed in experiments with a typical density of $\rho \sim 0.03$ kg/m^3 we obtain from Eq. (1) the effective gravity $\tilde{g} \sim 0.1$ m/s^2 (which is about 1% of g) and the surface tension $\alpha \sim 10^{-10}$ kg/s^2. The latter value is in good qualitative agreement with the observed $\alpha \sim (1$–$3) \times 10^{-10}$ kg/s^2, which we roughly estimate from $\alpha \sim M/\tau^2$. Here M is the total mass of the particles transported during the break-up of the lid during time τ. (An example used for this estimation is shown in Fig. 5(a).) Thus,

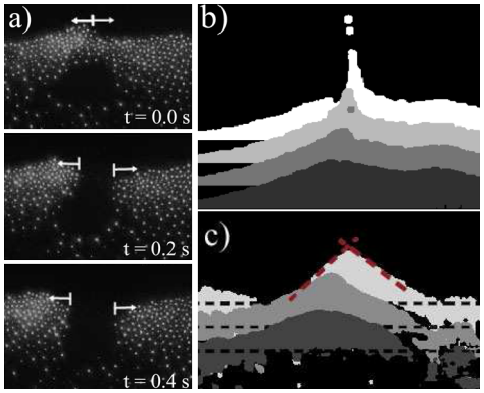

FIG. 5 (color online). Surface tension effects (6.8 μm particles, $\Delta T = 64.5$ K, $p = 18$ Pa, argon plasma). (a) Breaking up of a bubble lid (FoV 5×3 mm^2). The arrows indicate the size of the opening as well as the direction of particle motion. The vertical column shows three moments in time. We estimate the volume of the lid and the mean particle distance and calculate the surface tension from the total mass of the particles moved during the time needed for opening the bubble. Figures (b) and (c) show contours of the particle cloud at successive moments in time (gray scale and upwards displacement, marked by horizontal lines, indicate time) during (b) spray formation (FoV 9×4 mm^2, time step 0.48 s) and (c) evolution of a conic cusp (FoV 8×6 mm^2, time step 0.4 s). The red dashed lines show a Taylor cone with limiting angle of 98.6° [10].

capillary effects may indeed play a crucial role in the observed instability.

Note that the alternative mechanism that can in principle provide the selection of the most unstable mode—particle diffusion—is not sufficient to play any noticeable role in our experiments. Following [27], the wave number of the most unstable mode determined by diffusion is $k_{\max} \simeq (\frac{1}{16}\tilde{g}/D^2)^{1/3}$. By taking the value of the particle self-diffusion, $D \sim k_B T_g/m\gamma \sim 10^{-10}$ m^2/s [28] (T_g: gas temperature, m: microparticle mass) as the upper limit for D, we get $k_{\max} \gtrsim 2 \times 10^5$ m^{-1}, which corresponds to $\lambda_{\max}$ smaller than the interparticle distance. Another effect which could contribute to the confinement of the blobs are local space charges [29].

Capillary effects are known to be important for cusps [30,31]. The sharpness of the cusp tip is controlled by the capillary number $\mathcal{C} = \eta v/\alpha$, where η is the dynamic viscosity and v the stream velocity. Using the critical value of $\mathcal{C} = 0.25$ predicted in [30], ρ and α as given above, as well as a kinematic viscosity value $\nu = 1$ mm^2/s typical for complex plasmas [32,33], we obtain $v \sim 1$ mm/s, which is well in the interval of our observations. Figures 5(b) and 5(c) show the formation of a microparticle spray and a conic cusp, with the angle close to the limiting angle of a Taylor cone [10].

In conclusion, we investigated for the first time a new phenomenon occurring near the surface of fluid complex plasmas—the formation of microparticle bubbles, blobs, and surface cusps under the influence of thermophoresis. The behavior of microparticles is very similar to that observed in fluid drops and with sedimenting particles. The forces acting on the microparticles were analyzed and the velocity scaling with pressure was compared with a possible thermal creep flow inside the plasma chamber. Various effects have been observed that indicate the presence of surface tension, and qualitative agreement was found with the Rayleigh-Taylor instability.

This research was funded by DLR/BMWi Grant No. 50WP0203. The authors would like to thank P. Huber, M. Kretschmer, and R. Sütterlin for useful discussions.

*schwabe@mpe.mpg.de

[1] A. Wierzba, Exp. Fluids **9**, 59 (1990).
[2] G. Machu *et al.*, J. Fluid Mech. **447**, 299 (2001).
[3] D. Joseph *et al.*, Int. J. Multiphase Flow **25**, 1263 (1999).
[4] S. I. Han *et al.*, Phys. Rev. Lett. **87**, 144501 (2001).
[5] J. M. Nitsche and G. K. Batchelor, J. Fluid Mech. **340**, 161 (1997).
[6] J. F. Davidson *et al.*, Annu. Rev. Fluid Mech. **9**, 55 (1977).
[7] G. K. Batchelor and J. M. Nitsche, J. Fluid Mech. **278**, 63 (1994).
[8] H. R. Snyder *et al.*, Appl. Phys. Lett. **76**, 2511 (2000).
[9] D. Savignac and P. Leiderer, Phys. Rev. Lett. **49**, 1869 (1982).
[10] N. M. Zubarev, JETP Lett. **73**, 544 (2001).
[11] H. M. Thomas and G. E. Morfill, Nature (London) **379**, 806 (1996).
[12] P. K. Shukla and A. A. Mamun, *Introduction to Dusty Plasma Physics* (IOP Publishing, Bristol, 2001).
[13] V. E. Fortov *et al.*, Phys. Rep. **421**, 1 (2005).
[14] H.-Y. Chu *et al.*, Phys. Rev. Lett. **90**, 075004 (2003).
[15] H. M. Thomas *et al.*, New J. Phys. **10**, 033036 (2008).
[16] M. Schwabe *et al.*, Phys. Rev. Lett. **99**, 095002 (2007).
[17] H. Rothermel *et al.*, Phys. Rev. Lett. **89**, 175001 (2002).
[18] L. S. Pan *et al.*, J. Micromech. Microeng. **12**, 41 (2002).
[19] J. Goree *et al.*, Phys. Rev. E **59**, 7055 (1999).
[20] M. Rubin-Zuzic *et al.*, New J. Phys. **9**, 39 (2007).
[21] See EPAPS Document No. E-PRLTAO-103-024928 for a supplementary movie demonstrating the fluid behavior. For more information on EPAPS, see http://www.aip.org/pubservs/epaps.html.
[22] S. Chandrasekhar, *Hydrodynamic and Hydromagnetic Stability* (Oxford University, Oxford, 1961).
[23] E. H. Kennard, *Kinetic Theory of Gases* (McGraw-Hill Book Company, New York, 1938).
[24] S. Mitic *et al.*, Phys. Rev. Lett. **101**, 235001 (2008).
[25] C. P. Royall *et al.*, Phys. Rev. Lett. **98**, 188304 (2007).
[26] A. Wysocki *et al.*, Soft Matter **5**, 1340 (2009).
[27] R. E. Duff *et al.*, Phys. Fluids **5**, 417 (1962).
[28] E. M. Lifshitz and L. P. Pitaevskii, *Physical Kinetics* (Pergamon, Oxford, 1981).
[29] H. Totsuji *et al.*, Phys. Rev. E **72**, 036406 (2005).
[30] J.-T. Jeong and H. K. Moffat, J. Fluid Mech. **241**, 1 (1992).
[31] X. Cheng *et al.*, Nature Phys. **4**, 234 (2008).
[32] V. Nosenko and J. Goree, Phys. Rev. Lett. **93**, 155004 (2004).
[33] A. V. Ivlev *et al.*, Phys. Rev. Lett. **99**, 135004 (2007).